Dynamical scaling and fragmentation in viscous coarsening: An interrupted in-situ X-ray tomographic study

David Bouttes, Emmanuelle Gouillart, Elodie Boller, Davy Dalmas, Damien Vandembroucq

Dynamical scaling and fragmentation in viscous coarsening: An interrupted in-situ X-ray tomographic study

David Bouttes,[1] Emmanuelle Gouillart,[2] Elodie Boller,[3] Davy Dalmas,[2] and Damien Vandembroucq[1]

[1] *Laboratoire PMMH, UMR 7636 CNRS/ESPCI/Univ. Paris 6 UPMC/Univ. Paris 7 Diderot, 10 rue Vauquelin, 75231 Paris cedex 05, France*

[2] *Surface du Verre et Interfaces, UMR 125 CNRS/Saint-Gobain, 93303 Aubervilliers, France*

[3] *European Synchrotron Radiation Facility (ESRF), BP 220, 38043 Grenoble, France*

(Dated: September 6, 2013)

By means of computed X-Ray microtomography we followed the coarsening of a phase-separated ternary silicate glass in the liquid state. The volumes, surfaces, mean and gaussian curvatures of the domains of minority phase were measured after reconstruction of the 3D images and segmentation. We observed a growth law of the characteristic length scale $\ell \sim t$ consistent with the viscous coarsening of bicontinuous structure. All geometrical observables under study, either local or global, confirm the dynamical scaling hypothesis. A gradual fragmentation of the structure was observed in the less viscous phase and led to a power-law size distribution of isolated domains.

Introduction – The construction of a theoretical framework describing the phase separation of binary liquids[1–3] has been fueled by successive experimental developments. Up to the 90's, most experimental observations were performed in the Fourier space, with light or neutron scattering. Model systems were immiscible solutions [4, 5], and polymer blends [6, 7], or glasses [8]. These experiments confirmed that the dynamical scaling assumption is relevant for these systems, i.e. it is possible to rescale the structure factor by a unique length scale ℓ. This length increases with a power law: $\ell(t) \sim t^{\alpha}$, α depending on the growth regime [9]. More recent numerical simulations confirmed this scaling behavior, and provided some insights about the geometry in real space [10–12]. Meanwhile, new techniques of observation allowed to access direct space in experiments, such as scanning laser confocal microscopy: curvatures could be measured on phase-separated polymer blends [13, 14]. These observations are especially relevant to discuss the local mechanisms that govern the coarsening: pinch-off were for instance observed in a colloidal glass [15]. Recent predictions concerning statistical quantities such as size or surface distributions of domains also motivate the observation in real space [16, 17]. It has also been shown that the asymmetry of the two phases has a crucial influence on the morphology, as was shown by numerical simulations [18, 19] with a viscosity contrast. Experiments on polymers could also reveal the spectacular influence of visco-elastic effects [20]. However, the influence of a viscosity contrast has not yet been investigated in the hydrodynamical regime.

The development of X-Ray microtomography provides an appropriate tool to explore the 3-D geometry of phase separation, with submicron spatial resolution reached in Synchrotron facilities [21, 22]. Phase-separated polymer blends were already observed with phase-contrast imaging [23].

Glass-forming liquids offer an interesting opportunity to study phase separation [8]. A fast quench below the glass transition temperature enables to study the frozen structure in the solid state. Such an interrupted in-situ protocol naturally extends the variety of available techniques for characterization. Transmission and scanning electron microscopy, Raman Scattering and Atomic Force Microscopy have been used to characterize quantitatively phase separation in glasses [24–26]. We focus here on the late stage of spinodal decomposition after a deep quench into the unstable region, that produces interconnected structures. After the initial stage where the interfaces form, the growth can be described by a competition between the interfacial tension that favors the decrease of the surface area between each phase, and dissipative forces (viscosity, inertia).

In the following, we present first results on the observation of the coarsening in silicate melts at high temperature, using X-ray microtomography. After a description of the experimental system and the different steps of image processing, a 3D analysis of the main features of the coarsening stage will be given. The latter will be shown to enable to test (and confirm) the dynamical scaling hypothesis on a full set of morphological observables, far beyond the simple structure factor.

Materials and Method – *A model glass for phase separation* – Using the knowledge acquired in glass science [8], we designed a barium borosilicate glass to study phase separation. The composition of the glass was 57.1 %wt SiO_2, 23.3 %wt BaO, 18.9 %wt B_2O_3. Elaborated from raw materials, this composition was subsequently checked by wet chemical analysis. The glass decomposes into two phases: a minority barium-rich one, and a majority barium-poor, which ensures a good absorption contrast for X-Ray tomography, as barium is much more absorbing than the other elements. This system has a large metastable region which extends well above the liquidus [27, 28], which is appropriate to study the coarsening of a binary liquid. The viscosity contrast in the range of temperatures of our experiments is very high, the minority phase being much less viscous than the majority phase.

After elaboration an interconnected microstructure of typical size $\approx 1\,\mu$m was already present, because of the large temperature difference between the decomposition dome, and the glass transition temperature, that permitted phase separation even during a fast quench.

X-Ray tomography – A series of microtomography experiments were performed on the ID19 beamline at the European Synchrotron Radiation Facility (ESRF). 2 mm diameter samples were machined from the barium borosilicate glass and placed into fused silica tubes held by alumina crucibles. The glass samples were then observed during a heat treatment at a temperature corresponding to a liquid state (above T_G). Three experiments were done, at different temperatures: 1080 °C, 1130 °C and 1180 °C, using an interrupted in-situ protocol [22]. The samples were quenched at regular time intervals to room temperature. They were subsequently scanned, then heated again to the working temperature until the next quench. The typical time scale for the temperature changes is of the order of a few seconds. Because of the glassy nature of the material, and the relatively fast quench compared to the characteristic time of the domain growth, it is expected that the successive quenches should not influence the main features of the coarsening.

We used X-Ray radiation with a peak photon energy of 31 keV. For each scan, 900 X-ray radiographies were taken, from which the 3-D absorption field was reconstructed using the standard filtered-back projection algorithm, resulting in volumes of $512 \times 1024 \times 1024$ pixels. The spatial resolution was 0.7 µm, and the scan time was approximately 5 min.

Image processing – In order to study the geometrical and temporal evolution of each phase during the demixion process, the following method of segmentation was used. First, the reconstructed 3-D image was filtered to reduce the noise, by means of a Total Variation filter [29]. A fraction of the pixels could then be attributed unambiguously to one of the phases from the histogram of gray levels. Then, the remaining pixels were labelled using an anisotropic diffusion from the markers realized by the Random Walker algorithm [30]. The different domains could then be identified as the distinct connected components. Finally, we computed some geometrical characteristics: the volumes V_i, and surface S_i of all domains i from the statistics of neighboring configurations of 8-voxel cubes [31, 32], as well as the local curvatures on all points of the surfaces. The latter were obtained from a local fit of the interface by a quadric [33].

Results – After reconstruction and segmentation, the visual observation of a timeseries of images (Fig. 1) offers an intuitive idea of the coarsening. Most of the minority phase (barium rich), whose volume fraction is $35 \pm 5\%$, lies in a percolating network, but we observe also a growing fraction of isolated domains when time increases. The coarsening appears clearly: the width of the domains grows, and their surface gets smoother and smoother.

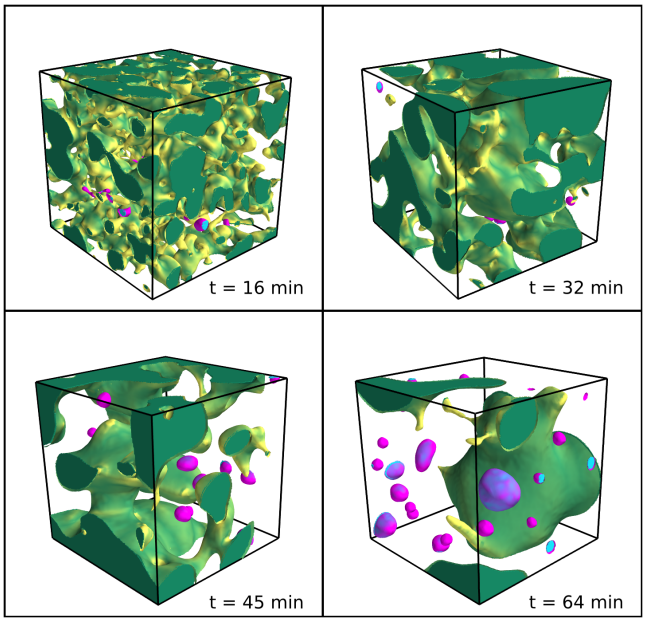

FIG. 1. 3D visualization[34] of the barium-rich phase, from scans after different times at 1130 °C (16, 32, 45, and 64 min). The color codes represent the absolute value of the mean curvature: shades of green for the percolating domain, shades of purple for isolated domains. The lateral size of the cube is 140 µm. The coarsening of the structure is accompanied by a fragmentation of the spanning cluster into isolated domains.

In the following, we first study quantities averaged over the whole volume, in analogy to previous experiments, to show the linear growth in time of the typical scale. Then, we give a more detailed account of the morphological features of the interconnected structure and their time evolution. Finally we characterize the development of a growing fraction of isolated domains.

Viscous coarsening – As mentioned before, various coarsening regimes have been proposed for phase separation, depending on the leading driving forces (diffusion, viscosity, inertia, etc.). The general scaling law is $\ell \sim t^{\alpha}$. Here, we define ℓ, the characteristic length scale, as three times the ratio between the total volume V_{tot} and the total surface area S_{tot} of the minority phase:

$$\ell = 3\frac{V_{tot}}{S_{tot}} \tag{1}$$

The prefactor 3 is chosen so that the characteristic length of a system of spheres of radius $r = \ell$ is exactly ℓ.

The time evolution of this length is plotted on Fig. 2 for T=1080 °C, 1130 °C, and 1180 °C, along with linear fits. As there was already a microstructure at the beginning of the experiment, $\ell(t = 0) \neq 0$. Our results are consistent with the linear growth proposed by Siggia [35] due to a hydrodynamic flow controlled by a competition between surface tension γ and viscosity μ:

$$\ell(t) \sim \frac{\gamma}{\mu} t.$$

This mechanism assumes that the Laplace pressure due to local curvatures induces a flow. It requires that the minority phase is interconnected, since in the case of isolated domains, the flow will stop as they approach a spherical shape. In the experiments most of the minority phase remains in the percolating domain (final volume ratio of about 75% to 90% depending on the experiment), so we do not expect a significant slowing down on the measure of ℓ. The coarsening is faster at higher temperature, due to the decrease of viscosity. Growth rates at different temperatures are consistent with an Arrhenius law (inset, Fig. 2).

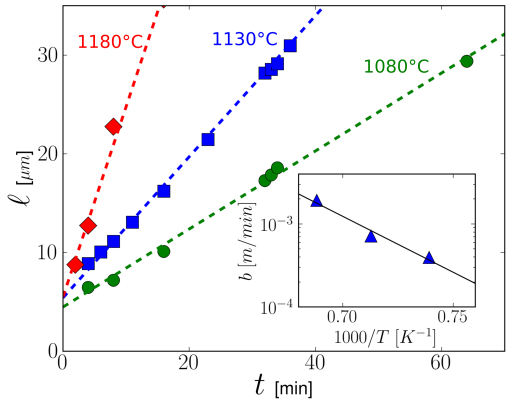

FIG. 2. Characteristic length ℓ vs time t, in for temperatures: 1080 °C (green circles), 1130 °C (blue squares), 1180 °C (red diamonds) for interrupted experiments. The dotted lines are linear fits. Inset: semi-log plot of the slopes of the linear fits b, as a function of the inverse temperature $1/T$.

Domain shape – Using the data from individual domains, we characterize their shape from the relation between their surface area and their volume. In order to characterize the shapes at different times, we normalize the volume V and the surface S of each domain, using the characteristic length scale ℓ:

$$v = \frac{V}{\frac{4}{3}\pi\ell^3} \quad ; \qquad s = \frac{S}{4\pi\ell^2}$$

The reduced volume v is plotted as a function of the reduced volume s for all domains and different times in Fig. 3. When close to a sphere, the volume of a domain should lie close to the black solid line representing the ideal sphere case. If more elongated, or ramified (see examples of domains in Fig. 3), it should have an excess of surface compared to a sphere, and hence get away from this line. According to this classification, we observe that most of the small domains are close to a spherical shape, whereas bigger domain deviate more and more as their volume increases. The dynamic lengthscale $\ell(t)$ separates a dominant population of small spheroidal clusters from a lower fraction of large ramified clusters.

Despite the poor statistic on large domains, a natural assumption would be to consider that the shape of large domains is inherited from the percolating structure, as isolated domains detached from it. They would subsequently change their shape towards spheres and/or fragment in more smaller domains. If we plot the normalized volume of the percolating domain v_p as a function of its scaled surface s_p, measured at different times and in boxes of different sizes within a given image, we find a linear relation: $v_p \sim s_p$, see Fig 3, dotted line. The large ramified domains shape follow also the same linear relation, and the crossover between the large and small domains corresponds well to the intersection of the two asymptotic regimes.

The excess surface observed for the percolating domain when approaching a box of size ℓ is simply due to sampling bias induced by the boundaries of the boxes. A non-trivial exponent could have been expected with an initial condition closer to the percolation threshold in three dimensions [16, 17].

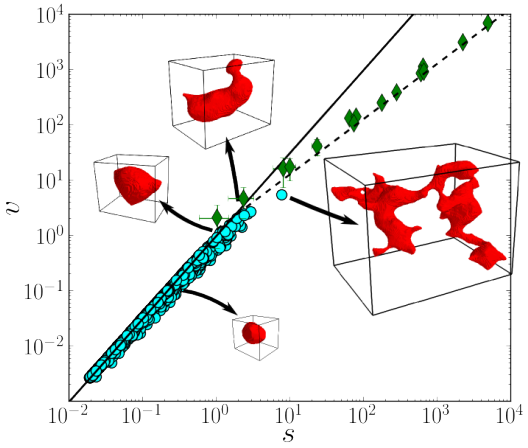

FIG. 3. Rescaled volumes v of the domains vs their rescaled surfaces s, for all isolated domains (cyan circles) and for the percolating domain (green diamonds) after 16, 32, 45, and 64 min at 1130 °C. The error bars indicate the standard deviation of the measures for all boxes of a given size. The black solid line is $v = s^{3/2}$ (ideal spheres), and the black dotted line is $v \sim s$. Some domains shapes are shown as examples.

Local curvatures – Another benefit of real space imaging is the possibility to access local geometrical observables such as local curvatures [14, 36] of the minority phase. In Fig. 4 we show the distributions of the mean curvature H and the Gaussian curvature K obtained after 16, 23, 32, 45, and 64 min at 1130 °C. As expected, both distributions get narrower and narrower along the coarsening process. The non-zero mean value of H is a consequence of the non 50-50 volume ratio of the phases. The asymmetry of gaussian curvatures reflects the topology of the structure: it indicates that the surface is dom-

inated by saddle-like shapes (negative gaussian curvature). The time evolution appears to be extremely well captured by means of a simple rescaling by the dynamic length:

$$P\left[H,\ell(t)\right] = \ell\Phi\left[H\ell(t)\right] \ ,$$
$$P\left[K,\ell(t)\right] = \ell^2\Psi\left[K\ell(t)^2\right] \ .$$

After rescaling (see Fig. 4) the distributions collapse onto a master curve. The excess positive gaussian curvature after rescaling at late times is the consequence of the fragmentation that form isolated domains (the logarithmic scale emphasizes this contribution).

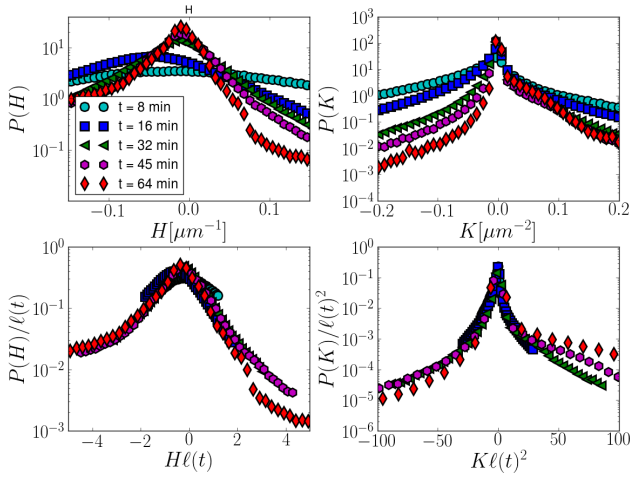

FIG. 4. Mean (H, left), and gaussian (K, right) curvatures distributions ; before (top), and after rescaling (bottom). After 8 (cyan circles), 16 (blue squares), 32 (green triangles), 45 (magenta hexagons), and 64 min (red diamonds) at 1130 °C.

Fragmentation – As was shown previously in Fig 1, isolated domains are not observed in the early stage of the experiment but they grow in number during the experiment, as a consequence of a fragmentation of the initial percolating structure. We show in Fig. 5 the time evolution of size distribution of the domains per unit volume $n_V = N(V)/V_{tot}$ (with $N(V)$ the number of domains of volume V, and V_{tot} the volume of the 3D image) measured at 1130 °C, plotted using logarithmic bins. Very small domains ($V_i < 1000$ voxels $\approx 700\ \mu\,\mathrm{m}^3$) are not shown here as it is very difficult to identify domains with linear sizes of the order of a few voxels. Using Monte Carlo simulations, we have also corrected the truncation bias affecting large domains touching the boundaries of the field of view.

We observe that more domains are present at longer times. In addition, we observe that the tail of the distribution changes with time, since large domains are observed at longer times. Despite the difficulty to obtain robust statistics for these large domains (only a few domains in the latest bins), the distribution seems to converge towards a power law distribution: $n_V \sim V^{-\beta}$ with an exponent $\beta \approx 1.7 \pm 0.1$.

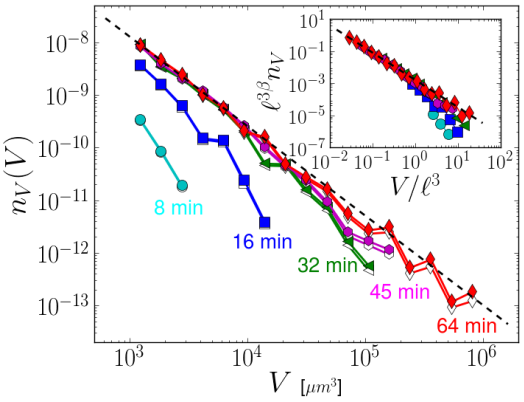

FIG. 5. Domains volumes distribution $n_v(V)$ (except percolating domain) after thermal treatment at T=1130 celsius during 8, 16, 32, 45 and 64 mn. The dotted line is $n_V \sim V^{-\beta}$, with $\beta = 1.7$. The open symbols show the size distributions before the correction due to the finite size of the field of view. The inset shows the same results after rescaling by the dynamical length $\ell(t)$.

The power law distribution seems to appear due to the formation of larger domains that detach from the percolating domain after some time, while the distribution of small domains remains fairly constant once they are formed. This could suggest that there exists an intrinsic size distribution that can be rescaled by the characteristic length ℓ. The difficulty to sample very small domains would hide the power law behavior for these domains at early times. Hence we tested the scaling (with $\ell(t)^3$ as characteristic volume):

$$n_V(V) \sim \ell^{-3\beta} f(\frac{V}{\ell^3}),$$

and obtained a reasonable collapse of the data as illustrated in Fig. 5 for the experiment performed at 1130 °C.

With the assumptions that domains of volume V detach at time $t \propto \ell(t) = V^{1/3}$, and that a larger number N_{break} of breaking events occur in a more ramified domain according to $N_{\mathrm{break}} \sim \ell^{-3}$, we obtain the distribution of domain volumes $n_V = N_{\mathrm{break}} \frac{dt}{dV} \sim V^{-5/3}$, consistent with our observation $\beta \simeq 1.7$.

Conclusion – The use of interrupted in-situ X-ray tomography gives access to a full tridimensional characterization of the coarsening process. Dynamic scaling was shown to account well for the evolution of all (global and local) geometrical observables. We observe a gradual fragmentation of the (minority) interconnected domain resulting in a complex multiscale microstructure, with a power-law distribution of isolated domain volumes, coexisting with the percolating phase. This fragmentation could also be renormalized using dynamical scaling.

Acknowledgments This work was supported by the ANR program "EDDAM" (ANR-11-BS09-027). Experiments were performed on line ID19 at ESRF in the framework of proposal HD501. We gratefully acknowledge the help of J. Grynberg, A. Lelarge, S. Patinet, F. Lechenault and J.-P. Valade for performing the experiments at the ESRF, as well as fruitful conversations with M.-H. Chopinet and L. Cugliandolo. We thank Yohann Bale for his help in sample preparation and Erick Lamotte for the glass elaboration.

[1] A. J. Bray, Advances in Physics **43** (1994).
[2] A. Onuki, *Phase transition dynamics* (Cambridge Univ. Press, 2002).
[3] R. W. Ballufi, S. M. Allen, and W. Craig Carter, *Kinetics of materials* (Wiley Interscience, 2005).
[4] Y. Chou and W. Goldburg, Physical Review A **20** (1979).
[5] N. Wong and C. Knobler, Physical Review A **24**, 3205 (1981).
[6] F. S. Bates and P. Wiltzius, The Journal of Chemical Physics **91**, 3258 (1989).
[7] M. Takenaka and T. Hashimoto, The Journal of Chemical Physics **96**, 6177 (1992).
[8] O. Mazurin and E. Porai-Koshits, *Phase Separation in Glass* (North-Holland, 1984).
[9] A. J. Bray, Philosophical transactions. Series A, Mathematical, physical, and engineering sciences **361**, 781 (2003).
[10] A. Wagner and J. Yeomans, Physical Review Letters **80**, 1429 (1998).
[11] N. González-Segredo, M. Nekovee, and P. Coveney, Physical Review E **67**, 1 (2003).
[12] S. Ahmad, S. Das, and S. Puri, Physical Review E **85**, 1 (2012).
[13] H. Jinnai, Y. Nishikawa, H. Morimoto, T. Koga, and T. Hashimoto, Langmuir **16**, 4380 (2000).
[14] C. R. Lopez-Barron and C. W. Macosko, Langmuir : the ACS journal of surfaces and colloids **25**, 9392 (2009).
[15] D. G. Aarts, R. P. Dullens, and H. N. W. Lekkerkerker, New Journal of Physics **7**, 40 (2005).
[16] A. Sicilia, J. Arenzon, A. J. Bray, and L. Cugliandolo, Physical Review E **76**, 1 (2007).
[17] A. Sicilia, Y. Sarrazin, J. Arenzon, A. J. Bray, and L. Cugliandolo, Physical Review E **80**, 1 (2009).
[18] K. Novik and P. Coveney, Physical review. E, Statistical physics, plasmas, fluids, and related interdisciplinary topics **61**, 435 (2000).
[19] K. Luo, W. Gronski, and C. Friedrich, Macromolecular Theory and Simulations **13**, 365 (2004).
[20] H. Tanaka, Journal of Physics: Condensed Matter **207** (2000).
[21] J. Baruchel, J.-Y. Buffiere, P. Cloetens, M. Di Michiel, E. Ferrie, W. Ludwig, E. Maire, and L. Salvo, Scripta Materialia **55**, 41 (2006).
[22] J. Y. Buffiere, E. Maire, J. Adrien, J. P. Masse, and E. Boller, Experimental Mechanics **50**, 289 (2010).
[23] A. Pyun, J. R. Bell, K. H. Won, B. M. Weon, S. K. Seol, J. H. Je, and C. W. Macosko, Macromolecules **40**, 2029 (2007).
[24] D. Dalmas, A. Lelarge, and D. Vandembroucq, Journal of Non-Crystalline Solids **353**, 4672 (2007).
[25] S. Schuller, O. Pinet, and B. Penelon, J. Amer. Ceram. Soc. **94**, 447 (2011).
[26] A. Hodroj, P. Simon, P. Florian, M.-H. Chopinet, and Y. Vaills, J. Amer. Ceram. Soc. **96**, 2454 (2013).
[27] E. M. Levin and G. M. Ugrinic, **25**, 47 (1953).
[28] E. M. Levin and G. W. Cleek, Journal of the American Ceramic Society **41**, 175 (1958).
[29] A. Chambolle, Journal of Mathematical Imaging and Vision **20**, 89 (2004).
[30] L. Grady, IEEE transactions on pattern analysis and machine intelligence **28**, 1768 (2006).
[31] C. Lang, J. Ohser, and R. Hilfer, Journal of microscopy **203**, 303 (2001).
[32] H.-J. Vogel, U. Weller, and S. Schlüter, Computers & Geosciences **36**, 1236 (2010).
[33] P. Sander and S. Zucker, IEEE Transactions on Pattern Analysis and Machine Intelligence **12**, 833 (1990).
[34] P. Ramachandran and G. Varoquaux, Computing in Science & Engineering **13**, 40 (2011).
[35] E. D. Siggia, Physical Review A **20**, 595 (1979).
[36] C. R. López-Barrón and C. W. Macosko, Soft Matter **6**, 2637 (2010).